References

ALBERTSSON, J. & ELDING, J. (1976). *Acta Cryst.* B32, 3066-3077.
ALLMANN, R. (1968). *Z. Kristallogr.* **126**, 417-426.
FEITKNECHT, W. (1933*a*). *Z. Kristallogr.* **84**, 173-176.
FEITKNECHT, W. (1933*b*) *Helv. Chim. Acta*, **16**, 427-454.
FRIDMAN, G. B. (1935). *Zh. Prikl. Khim. (Leningrad)*, **8**, 227-239.
GENTSCH, M. & WEBER, K. (1984). *Acta Cryst.* C40, 1309-1311.
GHOSE, S. (1964). *Acta Cryst.* **17**, 1051.
HILL, R. J. (1980). *Acta Cryst.* B36, 1304-1311.
HILL, R. J. (1981). *Acta Cryst.* B37, 1323-1328.
IITAKA, V., OSWALD, H. R. & LOCCHI, S. (1962). *Acta Cryst.* **15**, 559-563.
International Tables for X-ray Crystallography (1974). Vol. IV. Birmingham: Kynoch Press. (Present distributor D. Reidel, Dordrecht.)
JACOB, M. & RIQUIER, J. (1969). *J. Metall.* **9**, 127.
JOHNSON, C. K. (1976). *ORTEP*II. Report ORNL-5138. Oak Ridge National Laboratory, Tennessee.
KUHN, O. B. (1830). *J. Schweigger's*, **60**, 337.
PASCAL, P. (1962). *Nouveau Traité de Chimie Minérale.* Vol. V. Paris: Masson.
REINDEL, F. (1869). *J. Prakt. Chem.* **106**, 371.
SHELDRICK, G. M. (1976). *SHELX*76. A program for crystal structure determination. Univ. of Cambrige, England.
STÄHLIN, W. & OSWALD, H. R. (1970). *Acta Cryst.* B26, 860-863.
TREIMAN, A. H. & PEACOR, D. R. (1982). *Am. Mineral.* **67**, 1029-1034.
WADSLEY, A. D. (1955). *Acta Cryst.* **8**, 165-172.

Acta Cryst. (1986). B42, 39-43

The Imaging of Individual Cation Columns in f.c.c. Mixed Alloy Systems

By O. TERASAKI*

Department of Physical Chemistry, University of Cambridge, Lensfield Road, Cambridge, England

DAVID J. SMITH† AND G. J. WOOD†

High Resolution Electron Microscope, University of Cambridge, Free School Lane, Cambridge, England

(*Received* 4 *September* 1984; *accepted* 22 *August* 1985)

Abstract

Electron micrographs of an f.c.c. Au-Mn alloy, of nominal composition $Au_{79}Mn_{21}$, recorded at 500 kV and better than 2 Å point resolution, have demonstrated that it is possible to distinguish between *different* atomic columns of this material in thin specimen regions. These results have been confirmed by computer simulations which indicate that the conditions for imaging, namely the specimen thickness and the objective-lens defocus, are not critical. Some experimental images suggest that the occupation probability of separate columns in the beam direction might be determined although the sensitivity of the technique has not been examined. A small region of a novel superstructure, $Au_{14}Mn_4$, has been observed.

1. Introduction

Binary alloys, of the general formula $A_{1-x}B_x(x \leq \frac{1}{2})$, form a complex variety of superlattice structures, many of which have been investigated using the techniques of high-resolution electron microscopy (HREM) (for a recent review, see Watanabe & Terasaki, 1984). The basic structure of these alloys can be found by the usual diffraction methods so that the problem of determining their complete unit-cell structure is reduced to that of establishing the arrangement of *B* atoms. For superlattices based on the f.c.c. lattice, the projected atomic structure along the [001] zone axis can be represented as shown in Fig. 1. Since the basic unit-cell dimensions for most alloys are typically *ca* 4 Å, then microscope resolutions of better than 2 Å are required to separate columns (1) and (2) and better than 2·8 Å to separate columns (1) and (3). It should be noted that, despite a difference in projected separation, the atoms in columns (2) and (3) are equivalent nearest neighbours to those in column (1).

In order to form an ordered alloy structure, the interaction between nearest-neighbour *B* atoms should be repulsive. Thus, when the concentration of *B* atoms is $\frac{1}{4}$ or less, no nearest-neighbour *B*-*B* pairs are likely to exist. In this case, it is not necessary to resolve the fundamental lattice and both bright- and

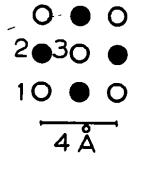

Fig. 1. Schematic showing the basic f.c.c. unit-cell structure of a binary alloy projected along [001]. Filled and empty circles are at different levels within the unit cell.

* Permanent address: Department of Physics, Faculty of Science, Tohoku University, Sendai 980, Japan.

† Present address: Centre for Solid State Science, Arizona State University, Tempe, AZ 85287, USA.

0108-7681/86/010039-05$01.50

dark-field microscope imaging techniques, including small apertures, can be used for structure determination. In the dark-field mode, image contrast is high, the image appearance is not critically dependent on objective-lens defocus or specimen thickness, and many superlattice structures, particularly in the AuMn system, have been determined using the technique (see, for example, van Tendeloo, de Ridder & Amelinckx, 1978). However, the atomic positions are not always reproduced correctly (Terasaki, Wood & Watanabe, 1984). Many superlattice structures have also been characterized using bright-field imaging in a high-voltage HREM (see, for example, Terasaki, Watanabe, Hiraga, Shindo & Hirabayashi, 1980, 1981; Hiraga, Shindo, Hirabayashi, Terasaki & Watanabe, 1980, 1982) since the so-called 'superstructure' images can be obtained without requiring the fundamental lattice to be resolved. Shindo (1982) was able to show that the brightness of the dots visible in these superstructure images was roughly proportional to the occupation probability of Mn atoms in the columns, if the relative intensities of the superlattice reflections were given kinematically. The changes of the images with defocus and specimen thickness have also been considered and the conditions appropriate for obtaining superstructure images discussed in detail (Hiraga, Shindo & Hirabayashi, 1981).

With an improvement in microscope resolving power to better than 2 Å, it becomes possible to resolve the basic lattice. The question then arises as to whether any information about the different site occupancies might be obtainable, for example by relating these to spot brightnesses as done for the superstructure images. This is particularly relevant for alloys with higher concentrations of *B* atoms where nearest-neighbour pairs of these atoms exist. This paper reports a preliminary investigation of this possibility using alloys based on the Au_4Mn structure where the Mn atoms align to form a column structure along the beam direction so that any differences in brightness should be due simply to the different atomic species (*i.e.* the extreme case of variable occupancy).

2. Methods

A sample of nominal composition $Au_{79}Mn_{21}$ was prepared for electron microscopy using the methods described previously (Terasaki *et al.*, 1981). High-resolution observations were made with the Cambridge University HREM (Smith *et al.*, 1982) at an operating voltage of 500 kV. Contrast-transfer calculations, confirmed by image simulation and optical diffractometry, indicate that at this voltage the microscope has an interpretable resolution (first zero crossing of contrast-transfer function) of slightly better than 2 Å. Image simulations were carried out with a local minicomputer (Saxton & Koch, 1982), using the multislice approach (Goodman & Moodie, 1974). Parameters used in the simulations were accelerating voltage 500 kV, spherical-aberration coefficient C_s = 2·7 mm, and focal spread 160 Å.

3. Results

(*a*) *Image simulations*

Images were simulated for the two-dimensional antiphase structure (2D-APS) which is shown schematically in Fig. 2, with only Mn-atom positions plotted (see Terasaki *et al.*, 1981). This structure consists of rhomboidal domains of 3×3 columns of Mn atoms having $D0_{22}$ structure, as shown by the dotted lines; each domain is separated by stepped antiphase boundaries where the arrangement of Mn atoms is $D1a$ structure.

A through-thickness (increments of 20·2 Å), through-focal (focal steps of 100 Å) series of images calculated for 500 keV electrons and $C_s = 2{\cdot}7$ mm is shown in Fig. 3. These show, for example, that at a thickness of 20·2 Å and defoci in the range −400 Å to −600 Å all the atomic column positions are resolved, with the Mn atomic columns imaged as brighter dots relative to the Au atomic columns. In contrast, they appear as darker white spots at a defocus of ~ −1000 Å. With increasing thickness, there are further specific defocus values where the Mn atomic column positions are clearly visible, *and* distinguishable from the Au columns. An interesting example is at a thickness of 60·7 Å where the Mn positions are imaged strongly as black spots over a 400 Å focal range, even though the individual Au columns are not separately imaged here. At thicknesses greater than about 80 Å second-order interference effects become much stronger and much of the image detail is expected to be on a considerably finer scale than the basic 2 Å interatomic detail.

(*b*) *Experimental observations*

High-resolution images of $Au_{79}Mn_{21}$ were recorded from thin crystal regions (thickness $H \leq 250$ Å) and

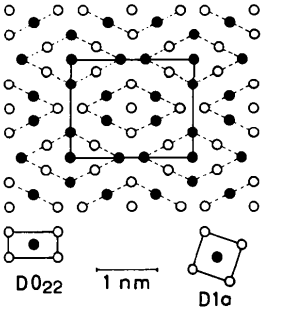

Fig. 2. Model of a two-dimensional antiphase structure (2D-APS) showing 3×3 rhomboidal domains of $D0_{22}$ structure (dotted), with antiphase boundaries. Only Mn atoms at two different levels are shown.

these indicated that there is considerable variation in the appearance of the material across a typical field of view as made apparent in the enlargements (hereafter labelled regions *A*, *B*, and *C*) in Figs. 4(*a*)-4(*c*) respectively. Corresponding optical diffractograms are shown in Figs. 5(*a*)-5(*c*). In Fig. 4(*a*), taken from a very thin area, the image basically consists of a square array of white dots having a separation of ~2 Å. In Fig. 4(*b*), the contrast of the bright spots varies substantially and they clearly now represent different atomic species. Indeed, from the arrangement of the spots it can be concluded that this region is primarily of the *D*1*a* structure and the excess Mn atoms are presumably accommodated by planar faults, such as that arrowed. There is a slight modulation in brightness of the spots at the boundary and this effect could be related to the occupation probability of Mn atoms, as discussed later in connection with conditions for 'superstructure' imaging. The contrast in Fig. 4(*c*), which corresponds to region *C*, is the same as that of the superstructure images reported previously (Hiraga *et al.*, 1980), *i.e.* only the Mn-atom columns are imaged at this thickness. The diffractograms also confirm these interpretations of the image features. Thus, Fig. 5(*a*) consists only of fundamental reflections, whereas Fig. 5(*b*) shows both fundamental and superlattice reflections with comparable intensities and in Fig. 5(*c*) the intensities of the superstructure reflections are much stronger than those of the fundamentals. Finally, note that the thickness at *B* and *C* could be well out of the range of the simulations of Fig. 3.

Further high-resolution micrographs which confirm the computer predictions concerning super-

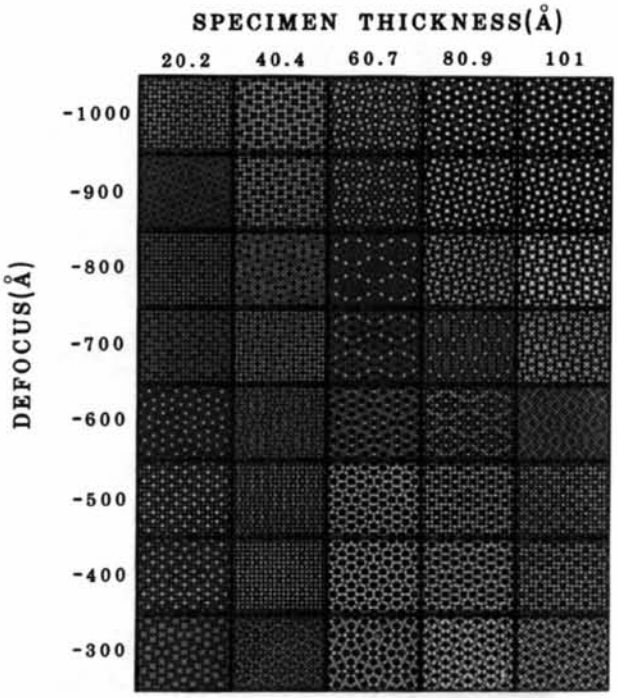

Fig. 3. Through-focal, through-thickness image calculations for $Au_{31}Mn_9$ with focus and thickness values as shown (500 kV, $C_s = 2.7$ mm, and focal spread $\Delta = 160$ Å). Mn atomic column positions are clearly visible at certain positions (see text).

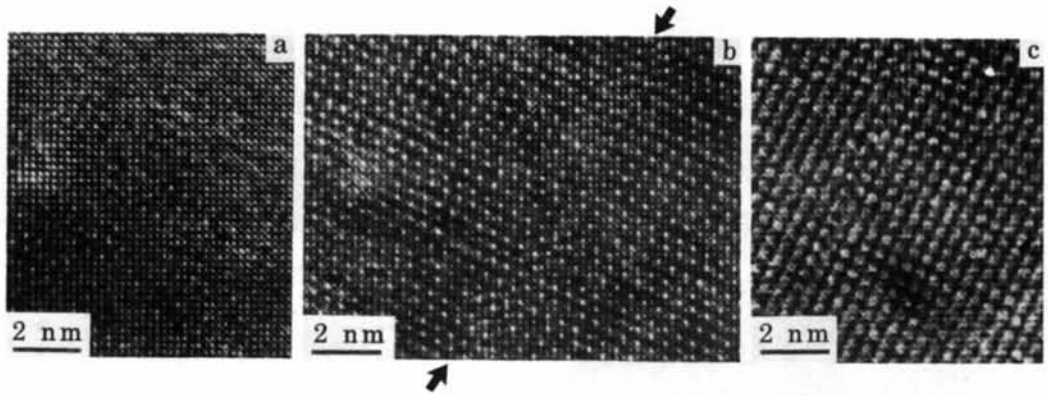

Fig. 4. (*a*)-(*c*) Enlargements from an image of $Au_{79}Mn_{21}$, recorded at 500 kV. Note planar fault arrowed in (*b*).

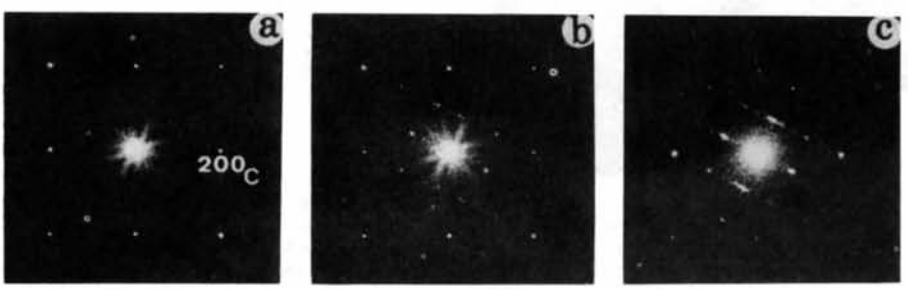

Fig. 5. (*a*)-(*c*) Optical diffractograms corresponding to Figs. 4(*a*)-4(*c*), respectively.

structure visibility are shown in Fig. 6. The image in Fig. 6(*a*) was recorded at close to the Scherzer defocus, the fundamental 2 Å cross-lattice is clearly discernible, and the superstructure can also be visualized to the extent that faults in the stacking sequence are clearly visible. In Fig. 6(*b*), recorded in a thicker region closer to the Gaussian (zero) focus, the image contrast is modulated by darker patches which, from the above simulations (Fig. 3), can be recognized as corresponding to the Mn-atom column positions.

Finally, Figs. 7(*a*) and 7(*b*) show high-resolution 'superstructure' images from a small region where the arrangement of white dots corresponding to Mn-atom columns is similar to one-dimensional long-period superstructures based on the Au_4Mn structure of *D*1*a*

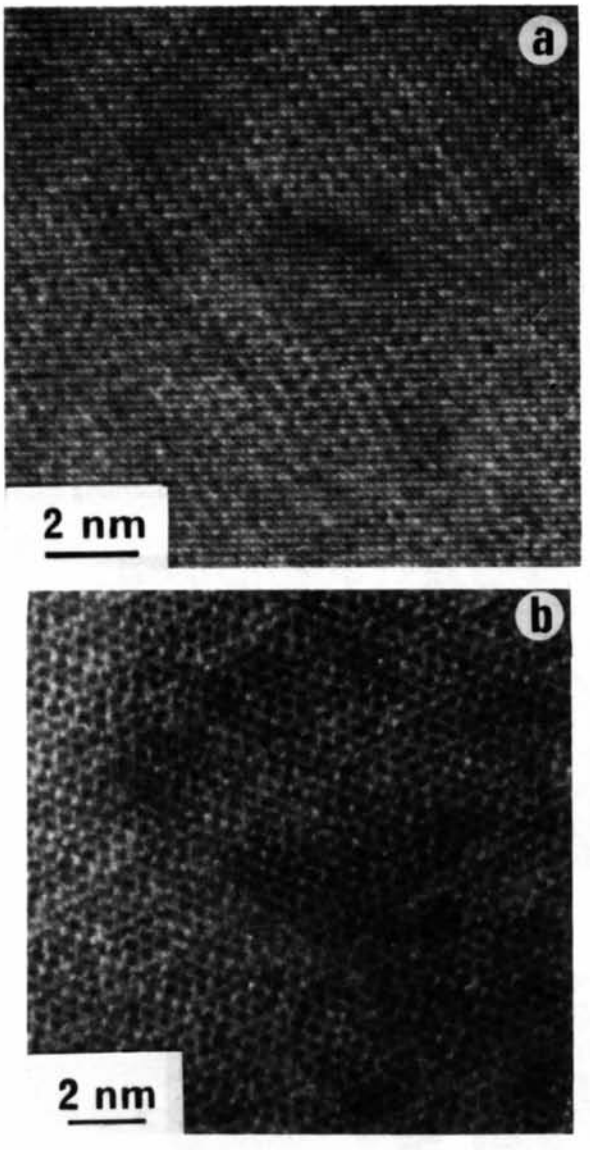

Fig. 6. (*a*) High-magnification image of $Au_{79}Mn_{21}$ from thin crystal region recorded at close to Scherzer defocus. Note the basic 2 Å cross-lattice and the superstructure variations. (*b*) Thicker crystal region near Gaussian focus. Dark-image modulations correspond to Mn atomic column positions.

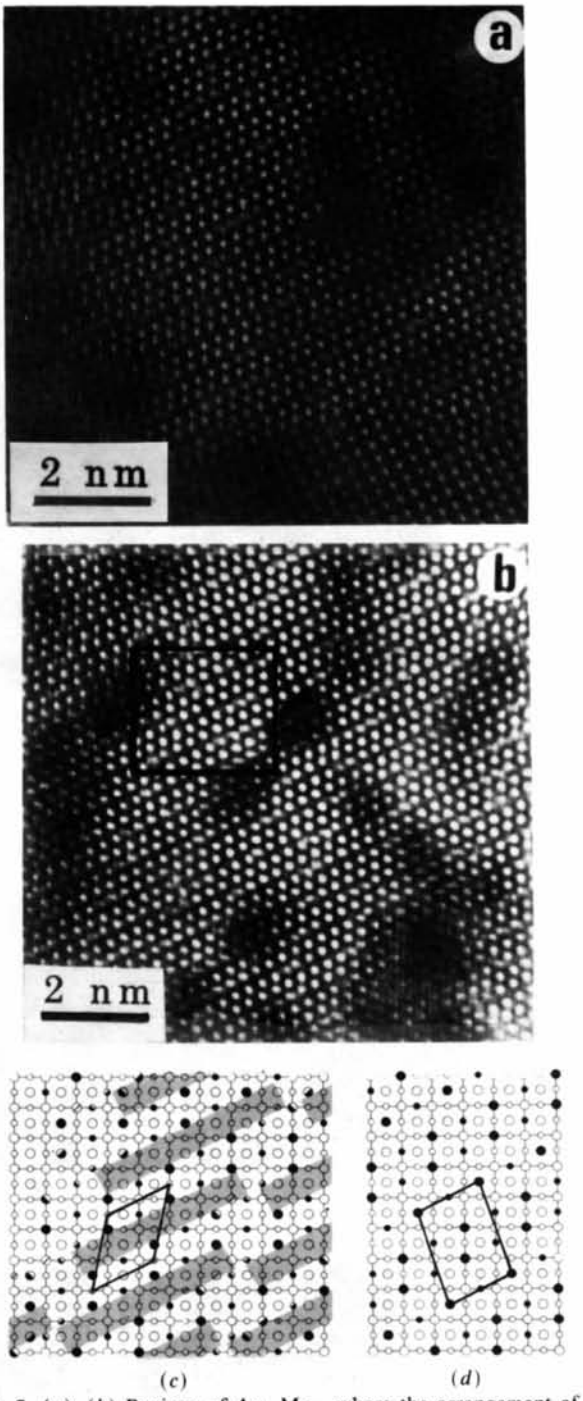

Fig. 7. (*a*), (*b*) Regions of $Au_{79}Mn_{21}$ where the arrangement of Mn atomic columns (white dot contrast) resembles that of the *D*1*a* long-period superstructure. (*c*) Schematic representation of area outlined in (*b*). Solid, half-filled and lined circles roughly indicate the Mn atomic occupation probability and the different circle sizes indicate different levels within the unit cell. Shaded regions show the *D*1*a*-type structure and the unit cell of $Au_{14}Mn_4$ is also outlined. (*d*) Model of $Au_{22}Mn_6$ with unit cell outlined.

type seen in $Au_{22}Mn_6$ (Hiraga *et al.*, 1982). In the present case, there is a sliding offset of Mn-column positions as indicated, for example, by the arrows in Fig. 7(*b*) and the width of *D*1*a* along the long-period axis is different. Careful observation of these images enables a schematic model for this lattice 'side-step' to be obtained, as drawn in Fig. 7(*c*) where the difference in brightness of spots is indicated by the lined, half-filled or solid circles (and the regions of *D*1*a* type are shown in screen-tone). The structure model of $Au_{22}Mn_6$ is also shown in Fig. 7(*d*) for comparison. Some apparent nearest-neighbour Mn–Mn pairs, the brightness of which is lower than that of other parts, are visible at the side-step. However, no nearest-neighbour Mn–Mn pairs are known to exist in this alloy. Moreover, the recorded image comes from the projection of the structure along the incident-beam direction. Thus, it can be concluded that the occupation probability of the Mn atoms in the columns is less than unity in order to avoid true nearest-neighbour Mn–Mn pairs, and this causes the lower contrast of the pairs, as discussed for the 'superstructure' image condition (Shindo, Hiraga & Hirabayashi, 1984). It is not possible to distinguish where the Mn atoms are located in the columns, whether there is perfect order along the tilt boundary or if the Mn atoms occupy the columns randomly along the beam direction. It should be noted that the superstructure shown in Fig. 7(*c*), which is effectively $Au_{14}Mn_4$, has not previously been reported.

OT expresses his thanks to Professor J. M. Thomas FRS, for the opportunity to work in Cambridge as Guest Research Fellow of the Royal Society. The support of the Science and Engineering Research Council, UK, is also acknowledged.

References

GOODMAN, P. & MOODIE, A. F. (1974). *Acta Cryst.* A**34**, 280–294.
HIRAGA, K., SHINDO, D. & HIRABAYASHI, M. (1981). *J. Appl. Cryst.* **14**, 185–190.
HIRAGA, K., SHINDO, D., HIRABAYASHI, M., TERASAKI, O. & WATANABE, D. (1980). *Acta Cryst.* B**36**, 2550–2554.
HIRAGA, K., SHINDO, D., HIRABAYASHI, M., TERASAKI, O. & WATANABE, D. (1982). *Acta Cryst.* A**38**, 269–274.
SAXTON, W. O. & KOCH, T. L. (1982). *J. Microsc.* **127**, 69–83.
SHINDO, D. (1982). *Acta Cryst.* A**38**, 310–317.
SHINDO, D., HIRAGA, K. & HIRABAYASHI, M. (1984). *Sci. Rep. Res. Inst. Tohoku Univ. Ser. A*, **32**, 32–45.
SMITH, D. J., CAMPS, R. A., COSSLETT, V. E., FREEMAN, L. A., SAXTON, W. O., NIXON, W. C., AHMED, H., CATTO, C. J. D., CLEAVER, J. R. A., SMITH, K. C. A. & TIMBS, A. E. (1982). *Ultramicroscopy*, **9**, 203–213.
TENDELOO, G. VAN, DE RIDDER, R. & AMELINCKX, S. (1978). *Phys. Status Solidi A*, **49**, 337–346.
TERASAKI, O., WATANABE, D., HIRAGA, K., SHINDO, D. & HIRABAYASHI, M. (1980). *Micron*, **11**, 235–240.
TERASAKI, O., WATANABE, D., HIRAGA, K., SHINDO, D. & HIRABAYASHI, M. (1981). *J. Appl. Cryst.* **14**, 392–400.
TERASAKI, O., WOOD, G. J. & WATANABE, D. (1984). *Mater. Res. Soc. Symp. Proc.* **21**, 253–257.
WATANABE, D. & TERASAKI, O. (1984). *Mater. Res. Soc. Symp. Proc.* **21**, 231–239.

Acta Cryst. (1986). B**42**, 43–50

The Determination of the Incommensurately Modulated Structure of Niobium Tetratelluride

BY SANDER VAN SMAALEN AND KLAAS D. BRONSEMA

Laboratory of Inorganic Chemistry, Materials Science Centre, University of Groningen, Nijenborgh 16, 9747 *AG Groningen, The Netherlands*

AND JAN MAHY

University of Antwerp (RUCA), Groenenborgerlaan 171, *B*-2020 *Antwerp, Belgium*

(*Received* 29 *October* 1984; *accepted* 16 *August* 1985)

Abstract

A complete analysis of the modulated structure of $NbTe_4$ is presented, using the newly developed formalism of de Wolff [*Acta Cryst.* (1974). A**30**, 777–785] and Yamamoto [*Acta Cryst.* (1982). A**38**, 87–92]. The diffraction pattern was measured at room temperature, including first-order and second-order satellites. The superspace group of the complete structure is $W^{P4/\frac{m}{1}\frac{c}{1}\frac{c}{1}}_{1}$. The final R_{F^2} value is 0·095 (0·044 for main reflections only), for a total of 3894 unique reflections (923 main reflections). The average structure found previously [Selte & Kjekshus (1964). *Acta Chem. Scand.* **18**, 690–696] is confirmed. In addition, the modulation wave is determined; it resides mainly on the Nb atoms, which have an amplitude of 0·33 Å. The results show that the displacements are correlated in such a way as to keep the Te–Te bonding distance constant and to minimize the variation in the shortest Nb–Te distance. It is found possible to refine at least

0108-7681/86/010043-08$01.50